

Electronic structure and spectra of ruthenium diimine complexes by density functional theory and INDO/S. Comparison of the two methods

S.I. Gorelsky*, A.B.P. Lever

Department of Chemistry, York University, 4700 Keele Street, Toronto, Ont., Canada M3J 1P3

Received 23 April 2001; accepted 15 June 2001

Abstract

Density functional theory calculations have been carried out on the series $[\text{Ru}(\text{bqdi})_n(\text{bpy})_{3-n}]^{2+}$ ($\text{bpy} = 2,2'$ -bipyridine, $\text{bqdi} = o$ -benzoquinonediimine) to explore the extent of coupling between metal 4d and ligand π and π^* orbitals. Time-dependent density-functional response theory (TD-DFRT) has been used to predict the complex electronic spectra which are compared with their experimental data. The main thrust of the paper is a comparison of these calculations with those carried out using Zerner's frequently used INDO/S method. Different procedures for the electron population analysis of molecular orbitals are described and discussed. The agreement in terms of orbital energies, orbital mixing and electronic spectra is remarkably good. This confirms that for these species, and probably for all non-solvatochromic species in general, INDO/S is a good model reproducing very well the results of the computationally much more demanding, but also more reliable TD-DFRT calculations. © 2001 Elsevier Science B.V. All rights reserved.

Keywords: Electron population analysis; Metal–ligand covalency; Time-dependent density-functional response theory; ZINDO

1. Introduction

Electronic coupling in transition metal complexes and the prediction of their electronic spectra has been a topic of our interest for a long time. We are interested in studying how the covalent bonding in inorganic complexes affects their electronic spectra and electrochemistry. Currently two theoretical methods, namely density functional theory (DFT) [1–11] and the semi-empirical INDO method [12–20] (or similar variants, as CINDO/CI [21–24]), are commonly used to analyze the electronic structure and spectra of transition metal complexes. From the 1970s until the present the INDO/S method developed for transition metal systems by M.C. Zerner was a primary tool to study transition metal systems. During the past ten years DFT has been remarkably successful at evaluating a variety of ground state properties with high accuracy. The time-dependent generalization of DFT (TD-DFT) offered a rigor-

ous route to calculate the dynamic response of the charge density. Combining this with the linear response theory allowed calculations of vertical electronic excitation spectra [4–10]. Several tests [6,10] have shown that current exchange-correlation functionals, including hybrid functionals, provide results for excitation energies superior to those obtained by standard ab initio techniques. The reliability of TD-DFT approach in obtaining accurate predictions of excitation energies and oscillator strengths is by now well documented. It has been successfully used to calculate the electronic spectra of transition metal complexes such as metal fluorides [25], metal carbonyls [26,27], nitrosyl complexes [28,29], quinone–catechol complexes [30], and metalloporphyrins [31]. We are interested to explore how different are the wavefunctions and properties of excited states obtained with DFT and TD-DFT from those obtained with INDO/S and whether the electronic spectra predicted by the two methods are similar or not. Certainly TD-DFT is regarded today as the more accurate computational method, but given the high computational costs involved, especially with larger molecules, it is

* Corresponding author. Fax: +1-416-736-5936.
E-mail address: serge@yorku.ca (S.I. Gorelsky).

important to know how close are the predictions from these two methods. In fact, large molecular systems such as multi-nuclear transition metal complexes are very demanding computationally and out of reach for DFT and TD-DFT calculations for now. INDO/S still has an important role to play for such systems and is computationally inexpensive—but how does it perform relative to TD-DFT?

Here, we study four ruthenium complexes, $[\text{Ru}(\text{bqdi})_n(\text{bpy})_{3-n}]^{2+}$ ($n = 0-3$, $\text{bpy} = 2,2'$ -bipyridine, $\text{bqdi} = o$ -benzoquinonediimine), to test and compare the performance of DFT and INDO/S methods. The diimine complexes of ruthenium have played an enormous role in the development of our understanding of the basic photochemistry and photophysics of transition metal systems. Among the fundamental questions that have been examined for these systems is the degree of spatial localization of transferred charge in the photoexcited states. We have previously studied these species using the INDO/S method [32,33] and now we want to verify our earlier conclusions by applying DFT and TD-DFT. This series has been chosen because it spans a range from relatively little Ru–ligand interaction (Ru–bpy) to very strong Ru–ligand (bqdi) interaction (or coupling).

One additional effect which must be considered is that solvent molecules interact strongly with highly charged ions, and these interactions are central to electron-transfer energetics.

2. Computational details

The DFT calculations presented in this article have been carried out using the GAUSSIAN-98 program [34]. Becke's three parameter hybrid functional [35] with the LYP correlation functional [36] (B3LYP) and an effective core potential basis set LanL2DZ [37–40] were employed in all the DFT calculations. The SCF convergence criterion was a change of less than 10^{-8} Hartree in the total energy.

Table 1
Calculated (B3LYP/LanL2DZ) and experimental Ru–N bond distances [45–47] in $[\text{Ru}(\text{bqdi})_n(\text{bpy})_{3-n}]^{2+}$

Complex	Ru charge ^a	$d(\text{Ru}-\text{N}(\text{bpy}))$ (Å)		$d(\text{Ru}-\text{N}(\text{bqdi}))$ (Å)	
		DFT	X-ray	DFT	X-ray
$[\text{Ru}(\text{bpy})_3]^{2+}$	0.891	2.100	2.056 ^b , 2.063–2.072 ^c	–	–
$[\text{Ru}(\text{bqdi})(\text{bpy})_2]^{2+}$	0.893	2.102, 2.119	2.06–2.09	2.036	2.00–2.04
$[\text{Ru}(\text{bqdi})_2(\text{bpy})]^{2+}$	0.902	2.114	–	2.046	–
$[\text{Ru}(\text{bqdi})_3]^{2+}$	0.912	–	–	2.054	–

^a Mulliken atomic charges, a.u.

^b $[\text{Ru}(\text{bpy})_3]_2(\text{PF}_6)_2$ structure [45].

^c $[\text{Ru}(\text{bpy})_3]_2[\text{Co}(\text{CN})_6]\text{Cl}\cdot 8\text{H}_2\text{O}$ structure [46].

The electronic spectra of these complexes were calculated with the INDO/S method [11–19] and time-dependent density-functional response theory (TD-DFRT) [4–10]. The INDO/S calculations have been carried out using HYPERCHEM 5.1 [41], utilizing the Ru atomic parameters from [42]. The overlap weighting factors σ – σ and π – π for INDO/S calculations were set at 1.265 and 0.585 [19], and the number of singly excited configurations used was 1250 (e.g. 25×25 occupied x virtual orbitals). The energies and intensities of the lowest 35 singlet–singlet transitions were calculated with TD-DFRT. The electronic populations of molecular orbitals were calculated using the AOMix program [44]. The absorption profiles of the complexes were calculated by the formula:

$$\varepsilon(E) = \sum_{(i)} a_i \exp(-2.773(E - E_i)^2 / \Delta_{1/2}^2),$$

$$a_i = 2.174 \times 10^9 f_i / \Delta_{1/2}$$

where the sum runs over all calculated transitions with energies, E_i , and oscillator strengths, f_i . So, the total integrated intensity under each absorption profile is equal to a sum of the oscillator strengths, $\sum_{(i)} f_i$. The half-bandwidths, $\Delta_{1/2}$, were assumed to be equal to 3000 cm^{-1} (a typical half-bandwidth value for electronic transitions of these complexes) for all electronic transitions.

3. Results and discussion

3.1. Structures

As can be seen from Table 1, DFT calculations with the B3LYP functional and LanL2DZ basis set are able to predict the structures of these complexes quite reasonably. The B3LYP/LanL2DZ calculations do overestimate the Ru–N bond lengths in $[\text{Ru}(\text{bpy})_3]^{2+}$ by 0.03–0.04 Å, but the local spin density calculations with the SVWN functional [48–51] and the same basis set gave underestimated Ru–N distances (2.023 Å). This is not surprising, because local spin density methods

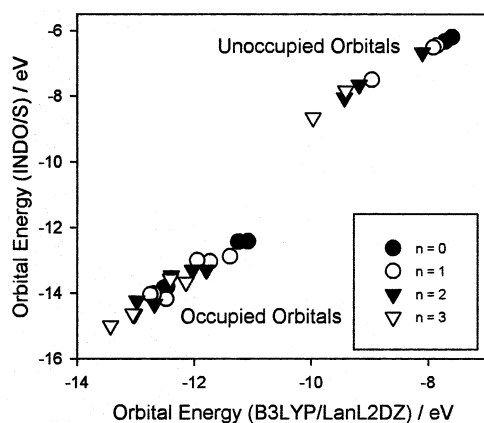


Fig. 1. Frontier orbital energies of $[\text{Ru}(\text{bqdi})_n(\text{bpy})_{3-n}]^{2+}$ complexes from the INDO/S and DFT (B3LYP/LanL2DZ) calculations.

usually lead to over-bound structures and give underestimated bond lengths in molecules and ions [1–3].

Calculated Ru–N (bqdi) distances are shorter than Ru–N (bpy) distances in $[\text{Ru}(\text{bqdi})_n(\text{bpy})_{3-n}]^{2+}$ complexes by some 0.06 Å, which is in good agreement with available X-ray data [47] (Table 1). The short Ru–N (bqdi) distances relative to Ru–N (bpy) distances reflect the stronger metal–ligand binding when the ligand is a strong π^* acceptor. As the number of bqdi ligands in $[\text{Ru}(\text{bqdi})_n(\text{bpy})_{3-n}]^{2+}$ complexes increases, the metal center become less electron-rich, back-donation per ligand decreases and the Ru–N bond distances (both Ru–bpy and Ru–bqdi) increase (Table 1).

3.2. Electronic structure and population analysis

From the beginning of the utilization of the DFT, the significance of the Kohn–Sham (KS) orbitals has been deemphasized. They have often been viewed as just an auxiliary construct, a necessary but not necessarily meaningful way to build up the all-important total electron density. Recently, Stowasser and Hoffmann [52] demonstrated that the shape and symmetry properties of the KS orbitals are very similar to those calculated by the Hartree–Fock and extended Hückel methods. We demonstrate here for the species under discussion that the atomic compositions of the KS orbitals are also very close to those from INDO/S calculations.

Like extended Hückel eigenvalues, those corresponding to KS orbitals often have smaller HOMO–LUMO gaps and are more consistent with excited-state energetics than are those from conventional ab initio or semi-empirical methods. This is also true for $[\text{Ru}(\text{bqdi})_n(\text{bpy})_{3-n}]^{2+}$ complexes. Their HOMO–LUMO gaps from B3LYP/LanL2DZ calculations are calculated to be 2.2–3.4 eV, which are two times smaller than the corresponding gaps derived from INDO/S calculations (5.0–6.1 eV). Both methods agree that the HOMO–LUMO gaps decrease as n increases from 0 to 3.

The energy order of the occupied orbitals is predicted, for the most part, to be the same by both the INDO/S and DFT methods (Fig. 1). It is also easy to spot that the molecular orbital energies from INDO/S calculations correlate linearly with the KS orbital energies. The order of a few frontier occupied orbitals is sometimes interchanged (Table 2), but this only happens when these orbitals are very close in energy (0.1 eV or less) and this is not a reason for a concern in the interpretation of the data. The order of the lowest empty orbitals is also very well preserved in calculations with both the methods. The three highest occupied molecular orbitals of $[\text{Ru}(\text{bqdi})_n(\text{bpy})_{3-n}]^{2+}$ are mainly Ru(4d) orbitals which would be the t_{2g} set in octahedral complexes. Their symmetries are $a_1 + e$ in the D_3 point group ($\text{Ru}(\text{LL})_3$ complexes) and $2a + b$ in C_2 ($\text{Ru}(\text{LL})(\text{LL}')_2$ complexes). For $n = 1$, one of these Ru orbitals has σ -symmetry, one has π -symmetry, and one has δ -symmetry with respect to the unique diimine ligand. The three lowest unoccupied orbitals are ligand π^* orbitals with symmetries $a_2 + e$ in D_3 and $a + 2b$ in C_2 . In the D_3 point group, there is no contribution from the d orbitals of the central atom to the LUMO which has a_2 symmetry and, thus, remains localized entirely on the ligands LL. For complexes with lower symmetry than D_3 , the LUMO can receive a contribution from the d orbitals of the central atom. Lying some 1.0–1.5 eV below the Ru(4d) occupied levels is a set of ligand π orbitals which have the same symmetries as the d orbitals of the central atom. These ligand orbitals are important in ruthenium–ligand bonding because they mix strongly with the Ru(4d) orbitals and, thus, affect the properties of the electronic ground state and also the corresponding excited states. Three lowest unoccupied and six highest occupied molecular orbitals are involved in electronic transitions of $[\text{Ru}(\text{bqdi})_n(\text{bpy})_{3-n}]^{2+}$ complexes in the visible and near UV-region. Since these orbitals determine the properties of the electronic excited states, it is important to analyze their orbital composition.

3.3. Methods to derive the extent of orbital mixing (atomic orbital contributions)

Within the MO-LCAO approximation, the wavefunction for the i th eigenstate of the molecule/ion can be written as

$$\psi_i = \sum_{(a)} c_{ia} \varphi_a$$

for an atom localized basis set $\{\varphi_a\}$.

In our previous studies we used semi-empirical zero differential overlap (ZDO) methods. Since the overlap between any two different basis functions, $S_{ab} = \langle \varphi_a | \varphi_b \rangle$, is neglected in these methods, the contribution of the a th atomic orbital (AO) to the i th molecular

orbital (MO) is simply equal to the square of the corresponding MO-LCAO coefficient, c_{ia}^2 . This is no longer the case if the overlap between atomic orbitals is non-zero. To analyze wavefunctions with non-zero overlap it is necessary to include the overlap population in the calculations. Several ways have been proposed in the literature to deal with overlap populations. The most popular and widely used procedure is Mulliken

population analysis (MPA) [53–56]. In MPA the overlap population is split equally between two atoms, so the contribution of the a th AO to the i th MO is equal to $c_{ia}^2 + \sum_{(b \neq a)} c_{ia}c_{ib}S_{ab}$ and the gross atomic population of atom A is

$$\sum_{(i)} n_i \sum_{(a)} \left(c_{ia}^2 + \sum_{(b \neq a)} c_{ia}c_{ib}S_{ab} \right)$$

Table 2
Irreducible representations, energies, and compositions (using MPA/MMPA/SCPA) of the frontier MOs of $[\text{Ru}(\text{bqdi})_n(\text{bpy})_{3-n}]^{2+}$ (INDO/S calculations were performed on DFT optimized structures)

$\text{Ru}(\text{bpy})_3^{2+}$									
	$\Gamma (D_3)$	B3LYP/LanL2DZ			INDO/S				
		$-\varepsilon$ (eV)	Ru (%) ^a	bpy (%) ^a	$-\varepsilon$ (eV)	Ru (%)	bpy (%)		
LUMO+1,2	e	7.59	6/6/6	94/94/94	6.20	6	94		
LUMO	a ₂	7.71	0/0/0	100/100/100	6.33	0	100		
HOMO	a ₁	11.08	83/77/78	17/23/22	12.43	84	16		
HOMO–1,2	e	11.25	76/71/75	24/29/25	12.45	77	23		
HOMO–3,4	e	12.46	0/0/0	100/100/100	13.81	0	100		
HOMO–5	a ₁	12.52	1/1/1	99/99/99	13.86	2	98		
$\text{Ru}(\text{bqdi})_2(\text{bpy})_2^{2+}$									
	$\Gamma (C_2)$	B3LYP/LanL2DZ				INDO/S			
		$-\varepsilon$ (eV)	Ru (%) ^a	bqdi (%) ^a	bpy (%) ^a	$-\varepsilon$ (eV)	Ru (%)	bqdi (%)	bpy (%)
LUMO+2	a	7.85	5/5/5	0/1/1	95/94/94	6.46	4	0	96
LUMO+1	b	7.91	3/3/3	1/1/1	96/96/96	6.52	3	2	95
LUMO	b	8.96	18/19/20	77/75/73	5/6/7	7.51	21	73	6
HOMO	a	11.39	57/52/57	37/40/33	6/8/10	12.89	67	25	8
HOMO–1	a	11.73	75/69/75	5/7/7	20/24/18	13.05 ^b	77	4	19
HOMO–2	b	11.95	59/57/61	29/28/24	12/15/15	13.01 ^b	55	35	10
HOMO–3	a	12.48	24/23/27	65/64/59	11/13/14	14.18 ^b	14	63	23
HOMO–4	b	12.69	1/1/1	1/1/1	98/98/98	14.03 ^b	1	1	98
HOMO–5	a	12.75	3/3/3	2/2/2	95/95/95	14.05 ^b	2	18	80
$\text{Ru}(\text{bqdi})_2(\text{bpy})_2^{2+}$									
	$\Gamma (C_2)$	B3LYP/LanL2DZ				INDO/S			
		$-\varepsilon$ (eV)	Ru (%) ^a	bqdi (%) ^a	bpy (%) ^a	$-\varepsilon$ (eV)	Ru (%)	bqdi (%)	bpy (%)
LUMO+2	b	8.10	4/4/4	1/2/2	95/94/94	6.67	4	1	95
LUMO+1	a	9.18	21/20/23	78/77/74	1/3/3	7.66	23	76	1
LUMO	b	9.43	11/10/13	86/86/83	3/4/5	8.05	12	84	4
HOMO	a	11.79	46/42/49	52/56/47	2/2/4	13.30 ^b	56	43	1
HOMO–1	b	12.03	36/32/41	58/61/54	6/7/5	13.30 ^b	56	35	9
HOMO–2	a	12.39	57/53/60	34/35/30	9/12/10	13.47	60	32	8
HOMO–3	b	12.68	25/24/30	68/67/63	7/8/7	14.33 ^b	6	92	2
HOMO–4	a	12.98	4/4/5	6/6/6	90/90/89	14.23 ^b	2	1	97
HOMO–5	a	13.02	33/33/37	57/56/52	10/11/11	14.64	22	75	3
$\text{Ru}(\text{bqdi})_3^{2+}$									
	$\Gamma (D_3)$	B3LYP/LanL2DZ			INDO/S				
		$-\varepsilon$ (eV)	Ru (%) ^a	bqdi (%) ^a	$-\varepsilon$ (eV)	Ru (%)	bqdi (%)		
LUMO+1,2	e	9.41	21/20/23	79/80/77	7.84	22	78		
LUMO	a ₂	9.97	1/0/0	99/100/100	8.66	0	100		
HOMO	a ₁	12.14	40/34/44	60/66/56	13.67 ^b	48	52		
HOMO–1,2	e	12.41	26/24/30	74/76/70	13.57 ^b	57	43		
HOMO–3,4	e	13.05	29/28/33	71/72/67	14.63	6	94		
HOMO–5	a ₁	13.43	44/43/49	56/57/51	14.99	28	72		

^a Atomic orbital contributions to frontier orbitals (derived using MPA, MMPA, and SCPA respectively, see the text).

^b The relative ordering of these orbitals differs in INDO/S and DFT calculations. The numbering of molecular orbitals from INDO/S calculations was adjusted to match those from DFT calculations.

where a runs over all atomic orbitals centered on the atom A, b runs over all atomic orbitals of the molecule, $n_i = 2, 1, 0$ are MO occupation numbers, and i runs over all molecular orbitals.

One variation on the Mulliken procedure is to divide the overlap population in a way that better reflects the non-equivalent sharing of electrons between non-equivalent atoms. Stout and Politzer [57] suggested that the overlap population is to be split between two atoms A and B based on the ratio of the corresponding MO-LCAO coefficients c_{ia} and c_{ib} :

$$c_{ia}^2 / (c_{ia}^2 + c_{ib}^2) \text{ for the atom A}$$

$$c_{ib}^2 / (c_{ia}^2 + c_{ib}^2) \text{ for the atom B}$$

This method is called a modified Mulliken population analysis (MMPA). In MMPA the contribution of the a th AO to the i th MO is equal to

$$c_{ia}^2 + \sum_{(b \neq a)} c_{ia}c_{ib}S_{ab}c_{ia}^2 / (c_{ia}^2 + c_{ib}^2)$$

Another way to partition electron density in molecules was proposed by Ros and Schuit [58] (SCPA). The overlap population is not considered and the contribution of the a th AO to the i th MO is assumed to be equal to:

$$c_{ia}^2 / \sum_{(b)} c_{ib}^2$$

where b runs over all atomic orbitals of the molecule.

All these electron population methods (MPA, MMPA, and SCPA) converge to the same results when the overlap between atomic orbitals diminishes. In a recent review of population analysis [59] it was incorrectly stated that the MMPA formula can be, *after some rearrangement*, transformed to the SCPA formula. In fact, SCPA is only equivalent to MMPA in a special case where molecular orbitals are represented as linear combinations of just *two* atomic orbitals with non-zero overlap:

$$\Psi_i = c_{ia}\varphi_a + c_{ib}\varphi_b$$

In all other cases SCPA and MMPA are not the same and give different answers as can be seen in Table 2. However, MMPA is not rotationally invariant [57b], what makes it useless in most applications. Generally, the electron populations computed by all three methods are consistent and do not differ much from each other. Large differences between MPA, MMPA, and SCPA results only occur when molecular orbitals are highly delocalized over different parts of a molecule.

The molecular orbital populations obtained with DFT (B3LYP/LanL2DZ) and INDO/S are in good agreement (Table 2) in spite of all the differences between these two methods, i.e. the extent of electronic coupling between metal and ligand orbitals predicted

by the two methods is remarkably similar. The results are especially close for the three lowest virtual and the three highest occupied molecular orbitals. Keeping in mind that these are the orbitals involved in electronic transitions in the visible and near-UV region, we can expect that the assignment of the absorption bands will be also similar for TD-DFRT and INDO/S methods.

The earlier INDO/S calculations [32,33] had emphasized the very extensive coupling between the metal 4d and both ligand π and π^* orbitals increasing in importance from bpy to bqdi. Delocalization through ruthenium is so extensive that these molecules behave much like organic delocalized species with ruthenium as part of the p framework. DFT paints a very similar picture where the extent of orbital mixing in each of the frontier orbitals in nearly all cases, is of very comparable magnitude to the INDO/S predictions despite the fundamental differences between the two approaches. Where differences occur, perhaps most marked with $[\text{Ru}(\text{bqdi})_3]^{2+}$, DFT predicts an even greater degree of covalency in the Ru–bqdi interaction. So our earlier conclusions are fully confirmed with these DFT calculations.

In $[\text{Ru}(\text{bqdi})_n(\text{bpy})_{3-n}]^{2+}$ π^* bqdi orbitals have Ru contributions from 10 to 23%, whereas bpy (π^*) orbitals have Ru contributions ranging from 3 to 6% (except LUMO of $n = 0, 3$ which is 0% Ru(4d) for reasons of symmetry). The Ru orbitals are highly mixed with the bqdi π systems, resulting in the Ru $d(t_{2g})$ levels containing only around 50% Ru character or even less. So, in fact, B3LYP/LanL2DZ calculations show more covalency in Ru–bqdi ligand bonding than INDO/S calculations do. This is especially evident for $[\text{Ru}(\text{bqdi})_3]^{2+}$ (Table 2). For HOMO – 1,2 and HOMO – 3,4 (both e symmetry) atomic orbital mixing between ruthenium and ligand orbitals seems much larger in DFT than in the INDO/S model. We will discuss this observation at the end of the paper.

4. Electronic spectra

The TD-DFRT and INDO/S methods were employed to evaluate the properties of the excited states of $[\text{Ru}(\text{bqdi})_n(\text{bpy})_{3-n}]^{2+}$ complexes. TD-DFRT provides a first principles method for the calculation of excitation energies within a density functional framework. The reliability of the TD-DFRT approach in obtaining accurate predictions of excitation energies and oscillator strengths is established [4–11,25–31]. TD-DFRT calculations give remarkably good results for low-lying excited states of clear valence type (contrary to ‘diffuse’ states), however, the performance of TD-DFRT may be significantly affected by the incorrect asymptotic behavior of the local spin density or generalized gradient potentials if the excited states have an excitation energy

Table 3
Comparison between experimental [47,63–65] and calculated electronic spectra of $[\text{Ru}(\text{bqdi})_n(\text{bpy})_{3-n}]^{2+}$

Experimental energy	TD-DFRT (B3LYP/LanL2DZ)			INDO/S		
	Energy	f^a	Assignment ^b	Energy	f^a	Assignment ^b
$[\text{Ru}(\text{bpy})_3]^{2+}$						
19.0	20.4	0.0004	H → L + 1,2(92%) d(Ru) → π*(bpy)	20.9	0.0006	H → L + 1,2(91%) d(Ru) → π*(bpy)
	20.4	0.0011	H → L (78%) d(Ru) → π*(bpy)	21.2	0.0006	H → L (89%) d(Ru) → π*(bpy)
22.2	22.1	0.015	H-1,2 → L (71%) d(Ru) → π*(bpy)	22.3	0.088	H-1,2 → L (72%) d(Ru) → π*(bpy)
23.4	23.3	0.22	H-1,2 → L + 1,2 (72%) d(Ru) → π*(bpy)	22.4	0.30	H-1,2 → L + 1,2(70%) d(Ru) → π*(bpy)
$[\text{Ru}(\text{bqdi})_2(\text{bpy})]^{2+}$						
13.3	11.2	0.0006	H → L (72%) d(Ru) → π*(bqdi)	10.2	0.0045	H → L (76%) d(Ru) → π*(bqdi)
	13.0	0.0010	H-1 → L (84%) d(Ru) → π*(bqdi)	11.5	0.0024	H-1 → L (72%) d(Ru) → π*(bqdi)
19.4	21.6	0.11	H → L + 2 (67%) d(Ru) → π*(bpy)			
	22.3	0.20	H-2 → L (46%) d(Ru) → π*(bqdi), H → L + 2 (24%) d(Ru) → π*(bpy)	20.9	0.65	H-2 → L (82%) d(Ru) → π*(bqdi)
22.8	24.4	0.063	H-1 → L + 1 (90%) d(Ru) → π*(bpy)	24.9	0.12	H-1 → L + 1 (79%) d(Ru) → π*(bpy)
$[\text{Ru}(\text{bqdi})_2(\text{bpy})]^{2+}$						
11.0	11.6	0.0052	H → L (81%) d(Ru) → π*(bqdi)	11.5	0.0083	H → L (67%) d(Ru) → π*(bqdi)
15.4	15.4	0.012	H-1 → L (73%) d(Ru) → π*(bqdi)	14.5	0.023	H-1 → L (74%) d(Ru) → π*(bqdi)
18.1	20.5	0.33	H-2 → L (48%) d(Ru) → π*(bqdi), H-1 → L + 1 (27%) d(Ru) → π*(bqdi)	18.3	0.82	H-2 → L (46%) d(Ru) → π*(bqdi), H-1 → L + 1 (30%) d(Ru) → π*(bqdi)
			22.1	23.1	0.091	H-3 → L + 1 (53%) π(bqdi) → π*(bqdi)
	25.8	0.15	H-1 → L + 2 (31%) d(Ru) → π*(bpy), H-5 → L + 1 (23%) π(bqdi) → π*(bqdi), H-4 → L + 1 (20%) π(bpy) → π*(bqdi)	23.7	0.25	H-2 → L + 1 (30%) d(Ru) → π*(bqdi)
$[\text{Ru}(\text{bqdi})_3]^{2+}$						
11.4	11.2	0.0020	H → L (90%) d(Ru) → π*(bqdi)	12.1	0.012	H → L (94%) d(Ru) → π*(bqdi)
15.2	15.3	0.12	H-1,2 → L (64%) d(Ru) → π*(bqdi)	14.5	0.29	H-1,2 → L (73%) d(Ru) → π*(bqdi)
20.6	21.2	0.40	H-3,4 → L (41%) π(bqdi) → π*(bqdi), H-1,2 → L + 1,2 (29%) d(Ru) → π*(bqdi)	18.9	1.24	H-1,2 → L + 1,2 (71%) d(Ru) → π*(bqdi)
			24.8	23.9	0.26	H-3,4 → L + 1,2 (88%) π(bqdi) → π*(bqdi)
	25.6	0.088	H-5 → L + 1,2 (87%) π(bqdi) → π*(bqdi)			

H = HOMO; L = LUMO

^a Oscillator strength.

^b Only the major parent one-electron excitations are reported. Their percentage contributions to wavefunctions of excited states are given in parenthesis.

higher than $-\epsilon_{\text{HOMO}}$ (the negative of the energy of the highest occupied KS orbital) and/or involve transitions to unbound virtual orbitals [7]. Although hybrid exchange-correlation functionals (including B3LYP) come closer to the correct Coulomb ($-1/r$) asymptotic behavior of the exchange-correlation potential, v_{xc} , they go asymptotically as $-a/r$ where a is some constant other than 1 [7]. In our B3LYP calculations, all the occupied electron levels for all the complexes have negative eigenvalues. The HOMO energies of the complexes are sufficiently low (between -11.1 and -12.1 eV) and the frontier unoccupied orbitals are bound, so there is no reason for concern in this case and TD-DFRT calculations should be successful.

The results of simulations of the electronic spectra of $[\text{Ru}(\text{bqdi})_n(\text{bpy})_{3-n}]^{2+}$ complexes are presented in Table 3 and Figs. 2–5. A detailed discussion of the

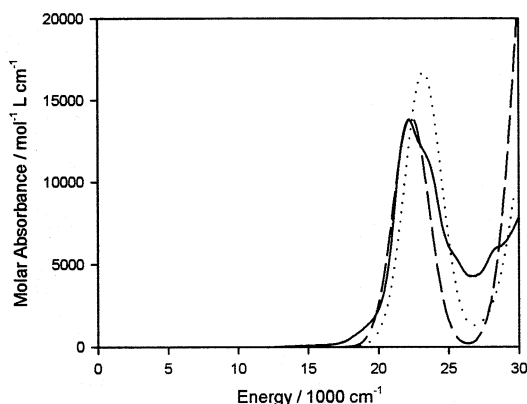


Fig. 2. Simulated (TD-DFRT, dotted line and INDO/S, hatched line) and experimental (solid line) electronic spectra of $[\text{Ru}(\text{bpy})_3]^{2+}$ complex. The experimental spectrum in CH_3CN . The intensities of electronic transitions from INDO/S calculations are reduced by a half.

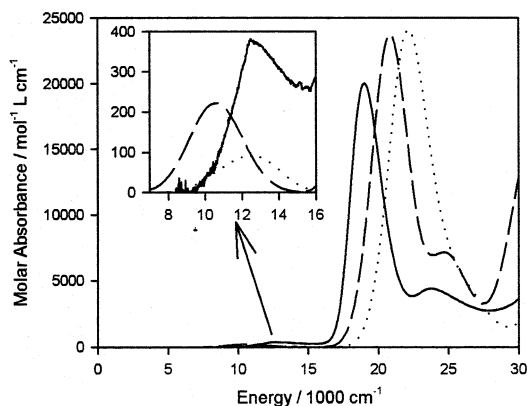


Fig. 3. Simulated (TD-DFRT, dotted line and INDO/S, hatched line) and experimental (solid line) electronic spectra of $[\text{Ru}(\text{bqdi})(\text{bpy})_2]^{2+}$ complex. The experimental spectrum in CH_3CN . The intensities of electronic transitions from INDO/S calculations are reduced by a half.

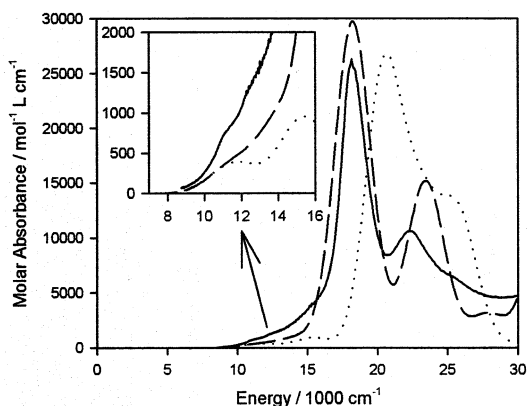


Fig. 4. Simulated (TD-DFRT, dotted line and INDO/S, hatched line) and experimental (solid line) electronic spectra of $[\text{Ru}(\text{bqdi})_2(\text{bpy})]^{2+}$ complex. The experimental spectrum in CH_3CN . The intensities of electronic transitions from INDO/S calculations are reduced by a half.

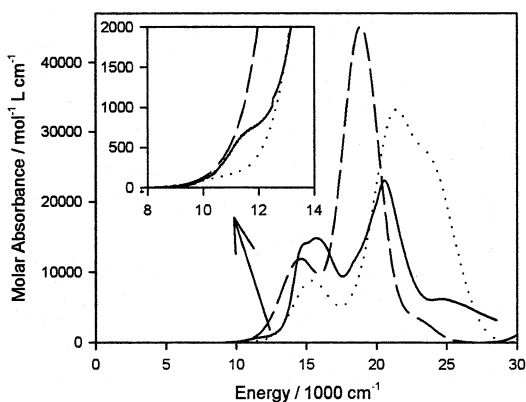


Fig. 5. Simulated (TD-DFRT, dotted line and INDO/S, hatched line) and experimental (solid line) electronic spectra of $[\text{Ru}(\text{bqdi})_3]^{2+}$ complex. The experimental spectrum in CH_3CN . The intensities of electronic transitions from INDO/S calculations are reduced by a half.

nature of the observed electronic transitions in these complexes has been previously reported in another publication [32]. Here, we discuss the features of the TD-DFRT and INDO/S calculations and how they relate to the experimental spectra of the complexes.

The spectrum of the ruthenium tris(bipyridine) complex, $[\text{Ru}(\text{bpy})_3]^{2+}$, is frequently used as a test species for theoretical methods and has been studied by different quantum-chemical models in the past. These studies include extended Hückel [60] and INDO/S [32,61] calculations. The multiplet structure of the ion has been also investigated with the local spin density approximation of DFT [62]. Unfortunately, the latter study did not include the calculation of the intensities of the electronic transitions.

The visible region spectra of the $[\text{Ru}(\text{bqdi})_n(\text{bpy})_{3-n}]^{2+}$ complexes exhibit several intense bands in the region $15\,000\text{--}25\,000\text{ cm}^{-1}$ region which were assigned to MLCT transitions from Ru d orbitals to π^* orbitals of bqdi and bpy ligands. For complexes with bqdi ligands, there is also an additional low-energy ($11\,000\text{--}12\,000\text{ cm}^{-1}$) and low-intensity band that is due to the HOMO \rightarrow LUMO excitation. Its appearance at such a low energy compared to the main absorption band is a very distinctive feature of complexes with the bqdi ligands whose provenance, arising from substantial Ru ($d\pi$)–ligand (π^*) mixing has been discussed [32,33].

As shown in Table 3, the TD-DFRT and INDO/S calculations give similar predictions which, for the most part, agree very well with the experimental data [47,63–65]. From Figs. 2–5 it is apparent that INDO/S consistently overestimates by a factor of ~ 2 the intensities of the bands in the spectra of the $[\text{Ru}(\text{bqdi})_n(\text{bpy})_{3-n}]^{2+}$ complexes. TD-DFRT calculations provide more reasonable absorption band intensities that lie closer to the experimental data.

4.1. $[\text{Ru}(\text{bpy})_3]^{2+}$

Both TD-DFRT and INDO/S give essentially the same predictions and assignments. The spectrum of the complex (Fig. 2) is dominated by one strong MLCT transition due to the HOMO $-1,2 \rightarrow$ LUMO $+1,2$ excitation. There is one transition with smaller intensity originating from weaker HOMO $-1,2 \rightarrow$ LUMO $+1,2$ excitation. According to INDO/S, its intensity is 30% of that of the main band. However, TD-DFRT calculations show that the intensity of the weak band is much smaller, only 7% of the intensity of the main band. There is another (small) discrepancy between TD-DFRT and INDO/S results. According to INDO/S, the energies of two MLCT bands are essentially the same, but TD-DFRT calculations show that these transitions are split by 1200 cm^{-1} . Since the experimental spectrum of the complex shows two transitions split by 1200 cm^{-1} , it appears that the TD-DFRT calculations make a more accurate prediction here than does INDO/S.

4.2. $[Ru(bqdi)_2(bpy)]^{2+}$

The spectrum of the complex (Fig. 3) is dominated by one strong MLCT ($Ru \rightarrow bqdi$) transition at $20\,000\text{ cm}^{-1}$ due to the $HOMO - 2 \rightarrow LUMO$ excitation. Both TD-DFRT and INDO/S give similar predictions and assignments. TD-DFRT simulations show that there is an additional electron excitation MLCT ($Ru \rightarrow bpy$), $HOMO \rightarrow LUMO + 2$, that contributes significantly (24%) to the electronic transition at $22\,300\text{ cm}^{-1}$ and also appears as an additional band at $21\,600\text{ cm}^{-1}$ with an intensity of 50% of the main MLCT band. However, the INDO/S method predicts that this $HOMO \rightarrow LUMO + 2$ excitation has a substantially lower intensity compared to the main MLCT band (only 7%) and occurs at higher frequencies ($27\,000\text{ cm}^{-1}$). The MLCT ($Ru \rightarrow bpy$) transition at $22\,800\text{ cm}^{-1}$ arises from the $HOMO - 1 \rightarrow LUMO + 1$ excitation and both TD-DFRT and INDO/S calculations give the same prediction and assignment for this band.

There are two weak transitions in the $10\,000\text{--}13\,000\text{ cm}^{-1}$ region due to $HOMO \rightarrow LUMO$ and $HOMO - 1 \rightarrow LUMO$ excitations ($Ru \rightarrow bqdi$). Both TD-DFRT and INDO/S give similar transition energies and the same assignments for these transitions. According to INDO/S and TD-DFRT, their total intensity is 0.5–1% of that of the main MLCT band at $20\,000\text{ cm}^{-1}$, in good agreement with the experimental data (Fig. 2).

4.3. $[Ru(bqdi)_2(bpy)]^{2+}$

The spectrum of the complex (Fig. 4) is dominated by one strong MLCT ($Ru \rightarrow bqdi$) transition at $18\,000\text{ cm}^{-1}$ due to the $HOMO - 2 \rightarrow LUMO$ and $HOMO - 1 \rightarrow LUMO + 1$ excitations. Both TD-DFRT and INDO/S give similar energies and the same assignments for this transition.

TD-DFRT and INDO/S calculations show that there are two weak transitions in at $11\,500$ and $15\,000\text{ cm}^{-1}$ due to $HOMO \rightarrow LUMO$ and $HOMO - 1 \rightarrow LUMO$ excitations ($Ru \rightarrow bqdi$). These transitions are observed in the experimental spectrum of the complex as the shoulders at $11\,000$ and $15\,000\text{ cm}^{-1}$. According to INDO/S and TD-DFRT, the intensities of these two transitions are 1–1.6% ($11\,500\text{ cm}^{-1}$ band) and 2.8–3.6% ($15\,000\text{ cm}^{-1}$ band) of the intensity of the main MLCT band at $18\,000\text{ cm}^{-1}$.

4.4. $[Ru(bqdi)_3]^{2+}$

The spectrum of the complex (Fig. 5) is dominated by two strong MLCT transitions at $15\,000$ and $20\,000\text{ cm}^{-1}$. The transition near $20\,000\text{ cm}^{-1}$ arises from the $HOMO - 1,2 \rightarrow LUMO + 1,2$ excitation (INDO/S). However, TD-DFRT simulations show that another excitation, $HOMO - 3,4 \rightarrow LUMO + 1,2$, is a major

contributor (41%) to this electronic transition, and the contribution from the $HOMO - 1,2 \rightarrow LUMO + 1,2$ excitation is smaller (29%). However, if we consider the atomic orbital contributions to the orbitals involved ($HOMO - 1,2$ and $HOMO - 3,4$), we shall notice that, in fact, both INDO/S and TD-DFRT calculations point to the similar assignment for this transition. The MLCT transition near $15\,000\text{ cm}^{-1}$ with smaller intensity originating from the $HOMO - 1,2 \rightarrow LUMO$ excitation. According to INDO/S and TD-DFRT, its intensity is 23–30% of that of the main band.

Both theoretical methods predict the existence of a low-intensity band near $11\,000\text{--}12\,000\text{ cm}^{-1}$ due to the $HOMO \rightarrow LUMO$ excitation and, indeed, this transition is observed in the experimental spectrum as a shoulder at $11\,400\text{ cm}^{-1}$.

One additional effect which needs to be considered is that solvent molecules interact strongly with highly charged ions, and such interactions are central to electron-transfer energetics. Solvation effects can be especially important for modeling the electronic spectra of highly polar solvents and/or solvents with hydrogen bonding. So, the agreement between calculated and experimental spectra might be regarded as surprising since the TD-DFRT calculation generates, in effect, a gas-phase spectrum. Certainly, charge transfer transitions are usually solvent sensitive [66]. However, the solvatochromism of the $[Ru(bqdi)_n(bpy)_{3-n}]^{2+}$ ions is very small [63,67,68]. Solvation of $[Ru(bqdi)_n(bpy)_{3-n}]^{2+}$ ions in solvents, such as acetonitrile, is rather weak, because of small charge-to-radius ratios for these complexes and the absence of any hydrogen-bonding interactions between the solute ions and the solvent molecules. Further, as the coupling between metal and ligand becomes more extensive ($Ru\text{--}bqdi$ complexes), the charge distribution in the excited state becomes more like the ground state, the net change in dipole moment between ground and excited state decreases, and solvatochromism diminishes further. Therefore this series of complexes is well suited for a gas-phase calculation, and gas-phase simulations are able to reproduce the experimental spectra very well.

This situation may not hold for the complexes containing ligands which are heavily solvated in solution (such as halogen ligands). For such complexes, we anticipate that simulated electronic spectra from TD-DFRT calculations will be significantly different from experimental data, reflecting the influence of the solvent on the electronic structure and spectra of such systems. Note, however, INDO/S calculations can still reproduce experimental spectra for 'solvatochromic atoms' reasonably well because the solvation effects are built in, or can be included, in INDO/S calculations by a suitable choice of the semi-empirical atomic parameters (such as valence state ionization potentials or one-center core integrals [17,19] and/or by changing the overlap

weighting factors). The INDO/S method has been parametrized to reproduce experimental spectra of transition metal complexes measured (in the most cases) in solution. So, INDO/S simulations should actually behave better with systems that do exhibit some solvatochromism, than pure phase simulations using TD-DFT. This observation can also explain the fact that DFT calculations indicate more covalency in metal–ligand bonding than do INDO/S calculations and X-ray absorption spectroscopic studies [69]. Due to electrostatic interactions, ionic structures are stabilized in polar solvents and in the solid state. As a result, the metal–ligand bond covalency is reduced. So, semi-empirical INDO/S and X-ray absorption spectroscopy will show less covalent metal–ligand bonds than gas-phase calculations using DFT.

5. Conclusions

The electronic spectra calculations for the $[\text{Ru}(\text{bqdi})_n(\text{bpy})_{3-n}]^{2+}$ complexes show that both INDO/S and TD-DFRT are remarkably accurate. The average deviation between the calculated and experimental transition energies is 1100 cm^{-1} (0.14 eV) for INDO/S and 900 cm^{-1} (0.11 eV) for TD-DFRT. Agreement between the two models is also exceptionally good. For $[\text{Ru}(\text{bqdi})_n(\text{bpy})_{3-n}]^{2+}$ complexes the INDO/S method provides reliable results close enough to those which could be obtained at much greater computational cost by TD-DFT. Therefore, we can trust INDO/S to do a good job with the larger molecules where density functional methods are still too costly. The symmetry properties and atomic orbital contributions of the KS orbitals are very similar to those calculated by the INDO/S method, and overall the KS orbitals are a good basis for the interpretation of the molecular orbitals and for understanding the electronic structure of the molecules, particularly with respect to the metal–ligand electronic interaction. The atomic orbital contributions of the KS orbitals are not very sensitive to the choice of the procedure for the electron population analysis (MPA, MMPA, or SCPA). The energy order of the occupied orbitals is in most cases in agreement between these two methods. Moreover, there is a linear correlation between the energies of KS orbitals from DFT calculations and the MO energies from INDO/S calculations (Fig. 1). All of this is really a tribute to the INDO/S parameterization.

Acknowledgements

We thank the Province of Ontario for an Ontario Graduate Fellowship (SIG) and NSERC (Ottawa) for financial support.

References

- [1] W. Kohn, A.D. Becke, R.G. Parr, *J. Phys. Chem.* **100** (1996) 12974.
- [2] A.D. Becke, in: D.R. Yarkony (Ed.), *Modern Electronic Structure Theory, Part II*, World Scientific, Singapore, 1995, p. 1022.
- [3] T. Ziegler, *Chem. Rev.* **91** (1991) 651.
- [4] M.E. Casida, in: D.P. Chong (Ed.), *Recent Advances in Density Functional Methods*, vol. 1, World Scientific, Singapore, 1995 (chap. 5).
- [5] M.E. Casida, in: J.M. Seminario (Ed.), *Recent Developments and Applications of Modern Density Functional Theory, Theoretical and Computational Chemistry*, vol. 4, Elsevier, Amsterdam, 1996, p. 391.
- [6] R. Bauernschmitt, R. Ahlrichs, *Chem. Phys. Lett.* **256** (1996) 454.
- [7] M.E. Casida, C. Jamorski, K.C. Casida, D.R. Salahub, *J. Chem. Phys.* **108** (1998) 4439.
- [8] R.E. Stratmann, G.E. Scuseria, M.J. Frisch, *J. Chem. Phys.* **109** (1998) 8218.
- [9] R. Bauernschmitt, R. Ahlrichs, F.H. Hennrich, M.M. Kappes, *J. Am. Chem. Soc.* **120** (1998) 5052.
- [10] M.E. Casida, C. Jamorski, K.C. Casida, D.R. Salahub, *J. Chem. Phys.* **108** (1998) 4439.
- [11] J. Juan, M.E. Casida, D.R. Salahub, *J. Mol. Struct. (Theochem)* **527** (2000) 229.
- [12] J. Ridley, M.C. Zerner, *Theor. Chim. Acta* **32** (1973) 111.
- [13] J. Ridley, M.C. Zerner, *Theor. Chim. Acta* **42** (1976) 223.
- [14] M.C. Zerner, G.H. Loew, R.F. Kirchner, U.T. Mueller-Westerhoff, *J. Am. Chem. Soc.* **102** (1980) 589.
- [15] W.P. Anderson, W.D. Edwards, M.C. Zerner, *Inorg. Chem.* **25** (1986) 2728.
- [16] W.P. Anderson, T.R. Cundari, M.C. Zerner, *Int. J. Quantum Chem.* **39** (1991) 31.
- [17] M.C. Zerner, in: K.B. Lipkowitz, D.B. Boyd (Eds.), *Reviews in Comp. Chemistry*, vol. 8, VCH, New York, 1991, p. 313 (chap. 2).
- [18] K.K. Stavrev, M.C. Zerner, T.J. Meyer, *J. Am. Chem. Soc.* **117** (1995) 8684.
- [19] M.C. Zerner, in: N. Russo, D.R. Salahub (Eds.), *Metal–Ligand Interactions*, Kluwer Academic, Amsterdam, 1996, p. 493.
- [20] M.C. Zerner, ZINDO Program, version 98.1, Quantum Theory Project, University of Florida, Gainesville, FL.
- [21] O.V. Sizova, V.I. Baranovskii, *J. Comp. Chem.* **16** (1995) 586.
- [22] O.V. Sizova, A.I. Panin, V.I. Baranovskii, N.V. Ivanova, *J. Struct. Chem.* **37** (1996) 171.
- [23] O.V. Sizova, A.I. Panin, N.V. Ivanova, *J. Struct. Chem.* **37** (1996) 181.
- [24] O.V. Sizova, V.I. Baranovskii, N.V. Ivanova, A.I. Panin, *Int. J. Quantum Chem.* **65** (1997) 183.
- [25] C. Adamo, V. Barone, *Theor. Chem. Acta* **105** (2000) 169.
- [26] S.J.A. van Gisbergen, J.A. Groeneveld, A. Rosa, J.G. Snijders, E.J. Baerends, *J. Phys. Chem. A* **103** (1999) 6835.
- [27] A. Rosa, E.J. Baerends, S.J.A. van Gisbergen, E. van Lenthe, J.A. Groeneveld, J.G. Snijders, *J. Am. Chem. Soc.* **121** (1999) 10356.
- [28] R.S. da Silva, S.I. Gorelsky, E.S. Dodsworth, E. Tfouni, A.B.P. Lever, *J. Chem. Soc. Dalton Trans.* (2000) 4078.
- [29] S.I. Gorelsky, A.B.P. Lever, *Int. J. Quantum Chem.* **80** (2000) 636.
- [30] S.I. Gorelsky, S.C. da Silva, A.B.P. Lever, D.W. Franco, *Inorg. Chim. Acta* **300** (2000) 698.
- [31] V.N. Nemykin, N. Kobayashi, *Chem. Commun.* (2001) 165.
- [32] S.I. Gorelsky, E.S. Dodsworth, A.B.P. Lever, A.A. Vlcek, *Coord. Chem. Rev.* **174** (1998) 469.
- [33] S.I. Gorelsky, A.B.P. Lever, *Coord. Chem. Rev.* **208** (2000) 153.

